Orientational dynamics of water confined on a nanometer length scale in reverse micelles

Howe-Siang Tan,[a] Ivan R. Piletic, and M. D. Fayer[b]
Department of Chemistry, Stanford University, Stanford, California 94305

(Received 27 December 2004; accepted 7 February 2005; published online 29 April 2005)

The time-resolved orientational anisotropies of the OD hydroxyl stretch of dilute HOD in H_2O confined on a nanometer length scale in sodium bis(2-ethylhexyl) sulfosuccinate (AOT) reverse micelles are studied using ultrafast infrared polarization and spectrally resolved pump-probe spectroscopy, and the results are compared to the same experiments on bulk water. The orientational anisotropy data for three water nanopool sizes (4.0, 2.4, and 1.7 nm) can be fitted well with biexponential decays. The biexponential decays are analyzed using a wobbling-in-a-cone model that involves fast orientational diffusion within a cone followed by slower, full orientational relaxation. The data provide the cone angles, the diffusion constants for motion within the cones, and the final diffusion constants as a function of the nanopool size. The two processes can be interpreted as a local angular fluctuation of the OD and a global hydrogen bond network rearrangement process. The trend in the relative amplitudes of the long and short exponential decays suggest an increasing rigidity as the nanopool size decreases. The trend in the long decay constants indicates a longer hydrogen bond network rearrangement time with decreasing reverse micelle size. The anisotropy measurements for the reverse micelles studied extrapolate to ~0.33 rather than the ideal value of 0.4, suggesting the presence of an initial inertial component in the anisotropy decay that is too fast to resolve. The very fast decay component is consistent with initial inertial orientational motion that is seen in published molecular-dynamics simulations of water in AOT reverse micelles. The angle over which the inertial orientational motion occurs is determined. The results are in semiquantitative agreement with the molecular-dynamics simulations. © *2005 American Institute of Physics*. [DOI: 10.1063/1.1883605]

I. INTRODUCTION

Water is fundamentally important in a multitude of physical and biological processes. Many of these processes involve water in confined nanoscopic environments, not in its bulk continuous form. Water confined on a nanometer length scale, i.e., "nanoscopic water" is important in chemistry,[1] biology,[2] and geology.[3] For instance, ion-exchange processes, important in analytical chemistry, are mediated by water in the confines of ion-exchange resins.[1] The dynamics of confined water in the vicinity of biomacromolecules are believed to be responsible for many biological functions, such as molecular recognition and enzymatic catalysis.[4] The water nanopools in reverse micelles are used as nanoreactors[5] and for hydration studies of enzymatic activity.[4]

The key feature of liquid water is its formation of dynamic hydrogen bond networks that are responsible for water's unique properties.[6] Bulk water dynamics occur over a range of time scales from tens of femtoseconds to several picoseconds.[7–14] Because water is found in many nanoscopic environments, an essential problem is the nature of water dynamics in nanopools and how nanoscopic water dynamics differ from those of bulk water.

Reverse micelles are widely used as model systems for studying water in confined nanoscopic environments.[15] Reverse micelles can be formed in a mixture of water, surfactant, and organic solvent. The water molecules are trapped in nanoscopic cavities (one to tens of nanometers in diameter) created by the surfactant molecules oriented so that their ionic or polar head groups point inward toward the aqueous phase. Sodium bis(2-ethylhexyl) sulfosuccinate (AOT) is a common surfactant used to make reverse micelles.

Many experiments on AOT reverse micelles have provided information on nanoscopic water properties and indirect information on dynamics. The optical experiments performed on AOT reverse micelles include linear infrared spectroscopy of the hydroxyl stretch,[16,17] librational motions,[18] and terahertz frequency spectroscopy of surface modes.[19] Time-resolved experiments have been performed using probe molecules to indirectly measure the dynamics of the surrounding water molecules. These experiments include visible fluorescence up-conversion spectroscopy[20,21] and mid-IR pump-probe spectroscopy.[22–24] Difficulties in interpreting the dynamical experiments arise from the uncertainties in the location of the probe molecules in the reverse micelle and the complexity of deciphering the influence of the water dynamics on the observable associated with the probe molecule. Nonetheless, these important experiments demonstrate that there are changes in the water dynamics that increase as the size of the reverse micelle water pool

[a]Permanent address: School of Physical and Mathematical Sciences, Nanyang Technological University, 1 Nanyang Walk, Singapore 637616.
[b]Electronic mail: fayer@stanford.edu

decreases. Transient IR spectra of the water hydroxyl stretch in reverse micelles have been measured,[25] but the picosecond time resolution used was too slow to examine the fundamental dynamics of the water molecules. Emphasis was on time scales of tens to hundreds of picoseconds. Very recently, an IR experiment examined the flow of vibrational energy from water nanopools in reverse micelles into the surrounding solvent.[26] Inelastic neutron-scattering experiments studied the dynamics of water in reverse micelles by obtaining the line shapes as a function of scattering angle.[27] The results were compared to the molecular-dynamics (MD) simulations.

Ultrafast IR spectrally resolved stimulated vibrational echo experiments have been used to directly examine the hydrogen bond dynamics of nanoscopic water in reverse micelles.[28–30] The results were compared to the experiments on bulk water and MD simulations of bulk water.[29,30] These series of experiments measure the time-dependent frequency fluctuations, i.e., spectral diffusion, of the OD stretch. The vibrational echo experiments provide insights into the hydrogen bond network evolution, and displayed a very pronounced dependence of the dynamics, particularly the long time scale dynamics, on the size of the water nanopool.

In this paper we present the studies of the orientational dynamics in water nanopools by observing the OD hydroxyl stretch of dilute HOD in water nanopools of AOT reverse micelles using ultrafast infrared spectrally resolved pump-probe experiments. The experiments measure the anisotropy decay as well as the vibrational lifetime. In contrast with bulk water, the anisotropy decays are not exponential, but fit well to a biexponential decay. A wobbling-in-a-cone model[31,42] is used to interpret the results. The orientational diffusion is initially restricted to a limited cone of angles. On a longer time scale complete orientational relaxation occurs. The cone angles, diffusion constants for motion in the cones, and the complete orientational diffusion constants are determined as a function of water nanopool size. It is observed that the initial anisotropy is not the ideal value of 0.4, but rather $\sim$0.33, with a small variation depending on the water nanopool size. The difference is assigned to a very fast initial inertial orientation motion that occurs on a time scale of $<$100 fs. The results of the measurements are compared to the MD simulations of orientational motion in reverse micelles.[27,32] The simulations display all of the features observed in the experiments and are in semiquantitative agreement with the experimental results.

II. EXPERIMENTAL PROCEDURES

The laser system used in the experiments consists of a home built Ti:Sapphire oscillator and a regenerative amplifier followed by an optical parametric amplifier (OPA) and difference frequency stage. The 800 nm $\sim$90-fs pulses pump the OPA containing a single 3-mm β-barium borate crystal that is double passed generating near-IR wavelengths (centered at wavelengths of $\sim$1.3 and $\sim$2.0 μm). A 0.5-mm $AgGaS_2$ crystal is used to difference frequency mix near the IR wavelengths to produce the $\sim$4-μm mid-IR pulses ($\sim$4 μJ/pulse). The pulses are characterized in the frequency domain by measuring their spectra with a monochromator. In all of the samples studied, the laser spectrum was tuned to match the peak of the OD stretch in the linear absorption spectrum. To determine the pulse duration in the sample, the time-delayed mid-IR pulses that are used in the experiment are cross-correlated in a nonresonant sample containing only CCl_4. The beams pass through the identical amount of optical material. The sign and magnitude of the chirp on the pulses are determined by frequency resolving the nonresonant signal in a monochromator [frequency-resolved optical grating[33] (FROG) experiment]. Calcium fluoride and germanium windows are placed in the beam prior to beam splitting to compensate the group-velocity dispersion. The results are 60-fs near transform limited pulses in the sample.

The IR pulses are split into pump and probe components with a relative intensity of 9:1. A polarizer (P1) is placed in the path of the probe beam to change the probe beam polarization to 45° relative to the pump beam. Both beams are then focused onto the sample using an off-axis parabolic reflector. Another off-axis parabolic reflector recollimates the probe pulse after the sample. The probe beam is then routed through a monochromator. A HgCdTe detector is placed at the monochromator exit slit to measure the frequency-resolved probe signal. The monochromator is set so that the detection wavelength matches the maximum of the OD absorption spectra of the different samples. Frequency resolution avoids the ambiguity introduced when signals from both the 0-1 and 1-2 vibrational transitions are observed simultaneously in a nonfrequency-resolved experiment. In addition, the presence or lack of a detectable wavelength dependence can provide useful information. A polarizer (P2) is placed after the monochromator just before the detector to selectively measure the parallel or perpendicular polarization components of the probe pulse. The polarizer before the HgCdTe detector has an extinction ratio of $\sim$120:1. The experiment is conducted as a function of the delay between the pump and probe pulses, t. A boxcar integrator measures the signal and is then sent to a lock-in amplifier. The pump pulse is chopped at a rate of 500 Hz. This frequency provides the lock-in frequency whereby the transient absorption signal can be obtained as $\Delta I_{\parallel}$ and $\Delta I_{\perp}$ for the parallel and perpendicular components, respectively. The lock-in signals are then normalized to the probe intensities of the two components ($I_{\parallel}$ and $I_{\perp}$), as measured on the HgCdTe detector. This gives the normalized parallel and perpendicular transient absorption signals $S_{\parallel}=\Delta I_{\parallel}/I_{\parallel}$ and $S_{\perp}=\Delta I_{\perp}/I_{\perp}$, respectively.

The pump-probe experiments were performed on the OD stretch of dilute HOD in H_2O (10% HOD in H_2O mixture) confined in monodispersed AOT reverse micelles. The low concentration of HOD in H_2O ensures minimal Förster energy transfer from an excited OD stretch to another OD. The average distance between a pair of HOD molecules at the concentration that we use is $\sim$6.7 Å compared to the Förster radius of $R_0=\sim$2.0 Å.[34,35] At a distance R_0, the transfer time equals the lifetime. The transfer rate falls off as $(R_0/R)^6$. Therefore, at the average separation, the transfer rate is approximately one thousandth of the lifetime decay rate, and the Förster transfer is negligible.

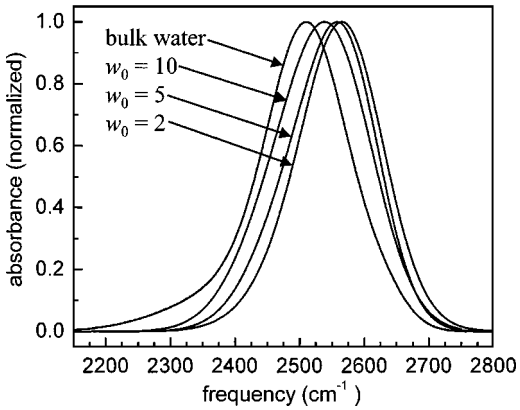

FIG. 1. Background-subtracted Fourier transform infrared (FTIR) spectra of the OD stretch of HOD in H_2O in bulk water and in AOT reverse micelles.

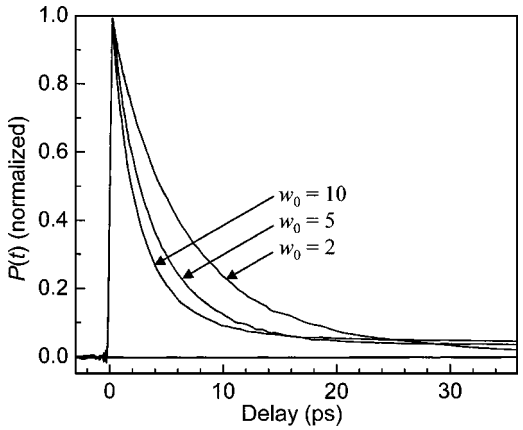

FIG. 2. Vibrational population relaxation of the OD stretch of HOD in H_2O in AOT reverse micelles (see text and Table I).

The reverse micelles were prepared in CCl_4 solvent, with $w_0=[H_2O]/[AOT]=10$, 5, and 2. The details of the preparation procedures are outlined in another publication.[30] Briefly, the reverse micelle samples were prepared by adding a measured volume of HOD/H_2O mixture to a stock solution of 1M AOT to give the desired w_0. The water content of the stock solution was determined by Karl Fisher titration, and the small water content of the stock solution was taken into consideration in determining concentration of water in the final samples. The size of the nanoscopic water pool at the center of the micelle can be assigned from w_0. For the w_0s studied, the nanopool sizes are approximately 4.0, 2.6, and 1.7 nm in diameter, containing ~1000, ~300, and ~50 water molecules, respectively.[36] Experiments were also performed on bulk water. The absorption spectra of the four samples are displayed in Fig. 1. The peak positions (cm^{-1}) and full width at half maximum (cm^{-1}) for the spectra of the OD stretch in bulk water and water nanopools in $w_0=10$, 5, and 2 reverse micelles are (2506, 170), (2539, 174), (2558, 160), (2566, 156), respectively. The spectra shift to higher frequency (blueshift) and become narrower with decreasing w_0.[16,17] The laser-pulse bandwidth spans the absorption spectrum of the sample under study. The samples were contained in a sample cell consisting of a Teflon spacer sandwiched between two pieces of 3-mm CaF_2 windows. The spacers used are 250 μm for the reverse micelles and 12 μm for bulk water. The optical densities are ~0.3 for all samples studied.

III. RESULTS AND ANALYSIS

The vibrational population dynamics $P(t)$ of the OD stretch of HOD in water, without contribution from orientational relaxation, was obtained using

$$P(t) = S_{\|}(t) + 2S_{\perp}(t). \tag{1}$$

The data for the water nanopools in the three reverse micelles are plotted in Fig. 2. The data are fit with an exponential decay and an offset. For HOD in bulk water it has been demonstrated in considerable detail that vibrational relaxation of the OD stretch leads to hydrogen bond breaking.[7–12] The hydrogen bond breaking produces changes in the spectrum that results in a long-lived nonzero pump-probe signal. The long-lived signal is either positive (residual ground state bleach) or negative (additional absorption) depending of the detection wavelength. At the center of the line, the long-lived signal is positive. In the reverse micelles, a detection wavelength-dependent long-lived signal is also observed in the $P(t)$ data. The long time scale nonzero signal is much smaller than the long-lived signal observed in bulk water and becomes smaller as the size of the nanopool decreases. The offsets for the reverse micelle sizes for $w_0=10$, 5 and 2 are ~4%, ~3%, and ~2%, respectively. Table I gives the decay constant T_1 for each size reverse micelle measured at its peak absorption wavelength. A detailed examination of the time dependence of the long-lived spectrum following vibrational relaxation will be presented subsequently.

The orientational anisotropy $r(t)$ is obtained from the time-resolved polarization selective pump-probe experiments by[37,38]

$$r(t) = \frac{S_{\|}(t) - S_{\perp}(t)}{S_{\|}(t) + 2S_{\perp}(t)} = 0.4C_2(t), \tag{2}$$

where $S_{\|}$ and S_{-} are the normalized parallel and perpendicular transient absorptions, respectively, as detailed in the experimental section. $C_2(t)=\langle P_2[\hat{\mu}(t)\cdot\hat{\mu}(0)]\rangle$ is the second-order Legendre polynomial of the transitional dipole moment unit vector orientation autocorrelation. At time $t=0$, $r(0)=0.4$, and $C_2(0)=1$.

The anisotropy data for the water nanopools in the reverse micelles with $w_0=2$ (circles), 5 (triangles), 10 (hexagons), and bulk water (squares) are shown in Fig. 3(a). In bulk water, the anisotropy decay is a single exponential with a decay constant of 1.9 ± 0.1 ps.[39,40] In contrast with bulk water, the anisotropy decays measured on the water nanopo-

TABLE I. Vibrational excited state lifetime decay constant, T_1 values.

Sample	T_1 (ps)
$w_0=2$	6.3
$w_0=5$	3.5
$w_0=10$	2.5
bulk water	1.5

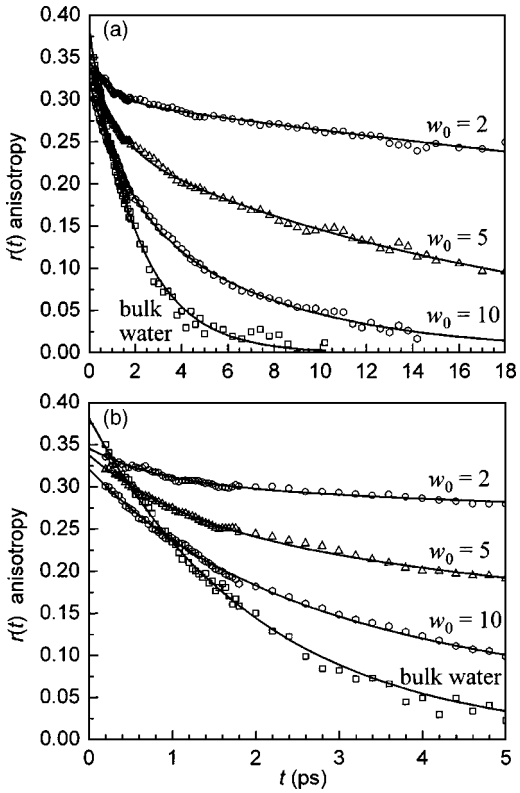

FIG. 3. Orientational anisotropy decays of the OD stretch of HOD in H_2O in bulk water and in AOT reverse micelles and biexponential fits (see Table II). (a) Long time scale. (b) Expanded time scale. Note the $t=0$ differences in $r(t)$ between the bulk water value ($\sim$0.39) and the reverse micelle values ($\sim$0.32–0.34).

ols in the three reverse micelles are not single exponential. The decays can be fit very well by a biexponential when $C_2(t)$ in Eq. (2) has the form

$$C_2(t) = A_1 \exp(-t/\tau_1) + A_2 \exp(-t/\tau_2). \tag{3}$$

The fitting begins at $t=200$ fs because of the large nonresonant signal centered at $t=0$ produced by the CCl_4 solvent. Although the pulses used in the experiments are $\sim$60 fs, the very strong nonresonant signal does not decay to zero until 200 fs. The time constants and amplitudes of the biexponential fits for the three w_0 values as well as for bulk water are listed in Table II.

The sum of the amplitudes of the biexponential fits to the anisotropy decays of all three reverse micelle samples add up to $\sim$0.33, but there are small differences for the three reverse micelles. Figure 3(b) displays the anisotropy data and fits on a shorter time scale so that the extrapolated values of the fits can be more clearly seen. The fact that the data do not extrapolate to 0.4 implies that there is a fast initial anisotropy decay that has occurred within the first 200 fs that is not measured in the experiments. The initial value of the anisotropy for bulk water is 0.385 ± 0.01, which is much closer to the ideal value of 0.4. Molecular-dynamics simulations show that bulk water has an initial inertial-libration contribution to the anisotropy decay.[13] This phenomenon has also been observed in recent ultrafast anisotropy studies of OH stretches in bulk water.[41] MD simulations show that water in reverse micelles also undergoes an initial fast decay of the anisotropy due to the similar inertial-librational motion preceding the orientational diffusion, but to a greater extent than in bulk water.[27] The inertial contribution will be discussed in more detail below. There are a number of clear trends of the observed biexponential decays that we can note here. First, the time constant of the longer decay increases with a decreasing size of the water nanopool. Second, the ratio of the amplitudes of the slow time decay to the fast time decay also increases as w_0 decreases.

TABLE II. Anisotropy decay parameters.

Sample	A_1	τ_1 (ps)	A_2	τ_2 (ps)
$w_0=2$	0.04	0.9 ± 0.2	0.30	78 ± 10
$w_0=5$	0.08	1.4 ± 0.2	0.25	19.5 ± 0.6
$w_0=10$	0.10	1.3 ± 0.2	0.22	6.2 ± 0.4
bulk water	0.385	1.9 ± 0.1		

The biexponential decaying anisotropy can be analyzed within an extended wobble-in-a-cone model.[31,42] In the standard model, two independent diffusion processes are proceeding simultaneously. The first, with a shorter correlation time, describes the motion of a restricted rotor, whereby the transition dipole moment can only undergo orientational diffusion within a cone of semiangle θ. The second longer correlation time accounts for the slower overall orientational relaxation without any angular restriction that results in complete orientational randomization. In this model the orientational correlation function is given by

$$C_2(t) = [Q^2 + (1-Q^2)\exp(-t/\tau_c)]\exp(-t/\tau_m), \tag{4}$$

where Q^2 is the generalized order parameter that describes the degree of restriction on the wobbling-in-the-cone orientational motion. Q^2 satisfies the inequality of $0 \leqslant Q^2 \leqslant 1$, where $Q^2=0$ describes unrestricted reorientation, while $Q^2=1$ is no wobbling-in-the-cone orientational motion. Q^2 is the amplitude of the slow decay in Eq. (4). It would be obtained from data by taking the slow decay amplitude of the $r(t)$ decay and multiplying it by 2.5 [see Eq. (2)]. τ_c is the time constant that describes the wobbling-in-the-cone motion. The time constant of the final diffusive full orientational relaxation is denoted τ_m, which, from Eq. (3), is the long time constant τ_2. τ_m gives directly the orientational diffusion coefficient of the angularly unrestricted orientation relaxation from the relation between the decay of the second Legendre polynomial and the diffusion constant,[43]

$$D_m = \frac{1}{6\tau_m}. \tag{5}$$

τ_c is obtained from the experimentally measured of τ_1 and τ_2 using the relation

$$\tau_c = (\tau_1^{-1} - \tau_2^{-1})^{-1}. \tag{6}$$

The cone semiangle θ is obtained from the order parameter Q^2 using[31]

$$Q^2 = \left[\tfrac{1}{2}(\cos\theta)(1+\cos\theta)\right]^2. \tag{7}$$

The wobbling-in-the-cone diffusion constant D_c is in turn related to τ_c and θ for $\theta \leqslant 30°$ by[31]

TABLE III. Cone angles and diffusion constants.

Sample	θ_{in}	θ_{tot}	D_c^{-1} (ps)	D_m^{-1} (ps)
$w_0=2$	19°	25°	38±2	470±60
$w_0=5$	20°	32°	31±2	117±3
$w_0=10$	22°	35°	25±2	37±2
bulk water				11.4±0.6

$$D_c \cong 7\theta^2/24\tau_c, \tag{8}$$

with θ in radians. In the experimental systems studied here, $\theta \leqslant 30°$, and Eq. (8) gives close to the correct values. In the simulations analyzed below, $\theta > 30°$, and the full expression for any value of θ must be used.[31]

$$D_c = \frac{x_c^2(1+x_c)^2\{\ln[(1+x_c)/2] + (1-x_c)/2\}}{\tau_c(1-Q^2)[2(x_c-1)]} + \frac{(1-x_c)(6+8x_c-x_c^2-12x_c^3-7x_c^4)}{24\tau_c(1-Q^2)}, \tag{9}$$

where $x_c = \cos\theta$. In the limit of $\theta = 180°$, i.e., there is no restriction to the orientational diffusion, $Q^2=0$ and $D_c = 1/6\tau_c$, as expected. The values reported for D_c^{-1} in Tables III and V were obtained using Eq. (9) in the manner presented below.

The analysis given above does not take into account that there is a very fast inertial component to the orientational relaxation. The very fast inertial motion partially randomizes the distribution before the onset of diffusive motion. The inertial motion produces an initial cone of orientations from which the wobbling-in-a-cone diffusion motion proceeds. The very fast inertial orientational decay produces a cone within a cone that needs to be treated to properly analyze the data and to extract additional information. The inertial component is too fast to measure because of the interference from the CCl_4 nonresonant signal. Simulations suggest that it is ~40 fs (Ref. 32) (see below). However, the amplitude of the inertial component is obtained from the experiments. The important quantity is the value of $C_2(t)$ following the inertial decay. That is the sum of the amplitudes A_1+A_2 [Eq. (3)] obtained form fitting $r(t)$ times 2.5, which is ~0.82, but varies somewhat with w_0.

To take into account the very fast inertial component of the decay, it is necessary to modify the wobbling-in-a-cone model given above. The inertial-librational motion is treated as an additional initial wobbling-in-a-cone motion that is independent of the subsequent longer time scale motion in a cone that is observed in the experiments on the ~1-ps time scale. Because the initial inertial decay is so much faster than the subsequent diffusive motions, the details of the inertial motion do not come into play. All that matters is that the inertial motion that produces an initial smaller cone of sampled angles is complete on a time scale that is much shorter than the following diffusive motion that samples the larger cone. Because the details of the functional form of the inertial decay are unimportant for the analysis presented here, we treat the inertial decay as exponential, although it must actually begin as a Gaussian decay since the slope of the correlation function C_2 is required to be zero at $t=0$. As shown in Appendix, the analysis yields a triexponential function,

$$C_2(t) = (1-T^2) \times \exp(-t/\tau_{in}) + T^2[S^2 + (1-S^2)\exp(-t/\tau_c)] \times \exp(-t/\tau_m). \tag{10}$$

The first term describes the decay of the initial very fast inertial component that is not directly observed in the experiments. The second term describes the biexponential curve that fits the experimental data [Eq. (3)].

There are two cones, the inertial cone and the total cone. The cone angle for each is calculated with the same formula, Eq. (7). The restricted orientational relaxation can be viewed as a decay to a plateau. The value of the plateau gives the cone angle. In the normal wobbling-in-a-cone, there is one plateau. In the absence of further orientational relaxation, the decay would be to a true plateau reflecting a spread of orientations to a particular value. However, in the single cone case described in Eq. (4), the plateau decays with the final diffusion process that leads to complete orientational randomization. In the experiments presented here, there are two plateaus. The inertial dynamics produces a decay to the first plateau. The decay from the first plateau is caused by diffusive wobbling-in-a-cone that leads to the second plateau, which in turn decays by the final diffusion process.

The inertial cone angle θ_{in} is determined by the initial value obtained by extrapolating $r(t)$ to $t=0$ [see Fig. 3(b)] and then multiplying this by 2.5 to get the value for the normalized correlation function. This value is T^2, the sum of the amplitudes of the biexponential fits, A_1+A_2 (see Table II), multiplied by 2.5. θ_{in} is obtained from Eq. (7) with $T^2 = Q^2$. While the first process is not diffusive, the cone angle is strictly geometric and determined by the level of the plateau. The total cone angle θ_{tot} describes the range of angles sampled by the combined inertial motion and the diffusive wobbling-in-a-cone motion. θ_{tot} is determined by the value T^2S^2 in Eq. (10), which is obtained from the $r(t)$ decay. T^2S^2 is A_2 multiplied by 2.5 to give the value in terms of the normalized correlation function.

Equations (4), (6), (7), and (9) would be used to determine the orientational diffusion constant for the wobbling-in-a-cone motion in the absence of inertial motion. For a single diffusive cone, the wobbling-in-a-cone motion causes the correlation function to decay from 1 to Q^2 [see Eq. (4)]. Here, the diffusive wobbling-in-a-cone motion causes a decay from T^2 to T^2S^2 [See Eq. (10)]. $T^2 = 2.5(A_1+A_2)$ and $T^2S^2 = 2.5A_2$. From these experimental values the effective cone angle is obtained by using S^2 in Eq. (7). This cone angle and τ_c [Eq. (6)] are used to determine the wobbling-in-a-cone diffusion constant D_c [Eq. (9)]. The calculated values of the inverse wobbling-in-a-cone orientational diffusion constant D_c^{-1} and the inverse overall orientational diffusion constant D_m^{-1} [Eq. (5)] are given in Table III. The orientational diffusion constant for bulk water is also given in Table III for comparison.

The values of the various parameters in Table III are size dependent. θ_{in}, the inertial cone angles, show a very small

increase with increasing water nanopool size that may be within experimental error. The trend in the total cone angle θ_{tot} also increases with increasing size, and this trend is outside of experimental error. The inverse wobbling-in-a-cone diffusion constant D_c^{-1} becomes faster as the nanopool size is increased. This trend is real; it is outside of experimental error. The most dramatic change is in the final complete diffusive orientational relaxation that randomizes the orientations. The inverse diffusion constant D_m^{-1} becomes much faster as the nanopool size increases. However, for $w_0=10$, D_m^{-1} is still ~ 3 slower than in bulk water.

The reverse micelles are themselves undergoing orientational diffusion in the solvent. It is important to estimate how much the orientational relaxation of the entire reverse micelle contributes, if at all, to D_m^{-1}. The Debye–Einstein–Stokes equation[44] describes the inverse orientational diffusion constant D_R^{-1} of a sphere in a solvent of viscosity η,

$$D_R^{-1} = \frac{8\pi\eta r^3}{kT}, \tag{11}$$

where k is the Boltzmann constant, r is the radius of the sphere, and T is the temperature in Kelvin. The radius of a $w_0=2$ AOT reverse micelle including the surfactant molecules is 1.9 nm.[45] Given the value for the viscosity of CCl_4 at 295 K of 0.969 cp,[46] D_R^{-1} is ~ 40 ns. This value is almost two orders of magnitude longer than the $D_m^{-1}=460$ ps that was found for the $w_0=2$ reverse micelle. Therefore, the contributions to the inverse diffusion constants reported in Table III from the orientational relaxation of the entire reverse micelles are negligible.

The data suggest that the orientation relaxation of water in the reverse micelle nanopools can be partitioned into two processes. The first is the local motions of water molecules within the hydrogen bond network. The second slower process involves the more global rearrangements of the constituent molecules of the network. In this picture, the cone semiangles θ_{tot} and the associated inverse diffusion constants D_c^{-1} reflect the first more local process while the inverse diffusion constants D_m^{-1} are measures of the second more global process.

Although there are constraints on the orientational diffusion of hydroxyls of a water molecule in a hydrogen bond network, the intrinsic flexibility of hydrogen bonds allows the hydroxyls to undergo directional fluctuations without breaking hydrogen bonds. The extent of the flexibility can be appreciated by studying the distribution of hydrogen bond angles (the angle made between the vector along the hydroxyl and the oxygen-to-oxygen vector between two adjacent hydrogen bonding molecules). Molecular-dynamics simulations on bulk water indicate that the hydrogen bond angles are distributed from 0° up to 40°.[13,14,47] Although not rigorously equivalent quantities, we may nonetheless compare this distribution of the hydrogen bond angles to the θ_{tot}. θ_{tot} takes into account both the initial fast inertial decay and the subsequent diffusive wobbling-in-a-cone motion. The values for θ_{tot} measured for the reverse micelles (Table III) are 25°, 32°, and 35° for $w_0=2$, 5, and 10, respectively. The increase θ_{tot} with increasing reverse micelle size may be due to the decreasing rigidity of the hydrogen bond network. In a constrained environment, the network cannot arrange in a geometrically optimum manner. Therefore, without breaking the hydrogen bonds, the fluctuations of the hydrogen bond angles of the constituent molecules are more limited in the smaller water nanopools and, hence, result in a smaller θ_{tot}. The same argument would explain the increasing inverse wobbling-in-a-cone diffusion constant D_c^{-1} with decreasing nanopool size.

The complete structural rearrangement of the hydrogen bond networks involves the rotation and translation of water molecules and consequently the breaking and formation of hydrogen bonds. With smaller reverse micelles, there are increasing geometric constraints to the rotational and translational freedom of the molecules undergoing the structural rearrangement. As the reverse micelle is made smaller, an increasing fraction of the water molecules interact with the head group boundary layer both physically and chemically. The inverse orientational diffusion constant for complete orientational relaxation D_m^{-1} reflects the time scale of the rearrangements and the underlying hydrogen bond breaking and reforming processes. There is a dramatic increase in D_m^{-1} as the size of the water nanopool decreases (see Table III). A similar trend is observed in the frequency-frequency correlation functions (FFCFs) of the OD stretch in water nanopools of reverse micelles measured with spectrally resolved stimulated vibrational echo experiments.[29,30] The FFCF measures the spectral diffusion of the OD stretch and the long time decay component is attributed to the hydrogen bond making and breaking processes.[12,13,48] The long decay constants of the FFCF measured for $w_0=10$, 5, and 2 are 5, 8, and 22 ps, respectively.[29,30] We can compare these values to the measured time constants of the slow reorientation τ_m [Eq. (5)] for water in reverse micelles $w_0=10$, 5, and 2 of 6, 20, and 78 ps, respectively. These values are not directly comparable because the vibrational echo experiments measure the FFCF while the experiments presented here measure $C_2(t)$. However, the trend may suggest that there are the same underlying physical processes, i.e., breaking and making of hydrogen bonds, responsible for the slowing observed in both types of experiments as the water nanopool size gets smaller. The trend of slower reorientation of the water molecules with decreasing reverse micelle size is also consistent with the experiments on probe molecules using visible fluorescence up-conversion spectroscopy[20,21] and mid-IR pump-probe spectroscopy.[22–24]

Although there are many MD simulations of bulk water, MD simulations of water in reverse micelles is still a relatively sparse field. The most comprehensive MD simulation of the dynamics of water confined in different sizes of model AOT reverse micelles has been performed by Ladanyi and co-workers.[27,32] Figure 4 displays the results of simulations of $C_2(t)$ from the MD simulations (solid curves) for reverse micelle sizes of $w_0=2.5$ and 5 (Ref. 27). [Figure 12 of Ref. 27 depicts the $\ln[C_1(t)]/[l(l+1)]$ calculated for $w_0=5$. For Fig. 4, we obtained the $C_2(t)$ values for $w_0=5$ and 2.5 from Ladanyi and co-workers simulated in the same study but not depicted in Ref. 27]. The simulations shown in Fig. 4 are the averages over all water molecules in the reverse micelles. When the water molecules were subdivided into two suben-

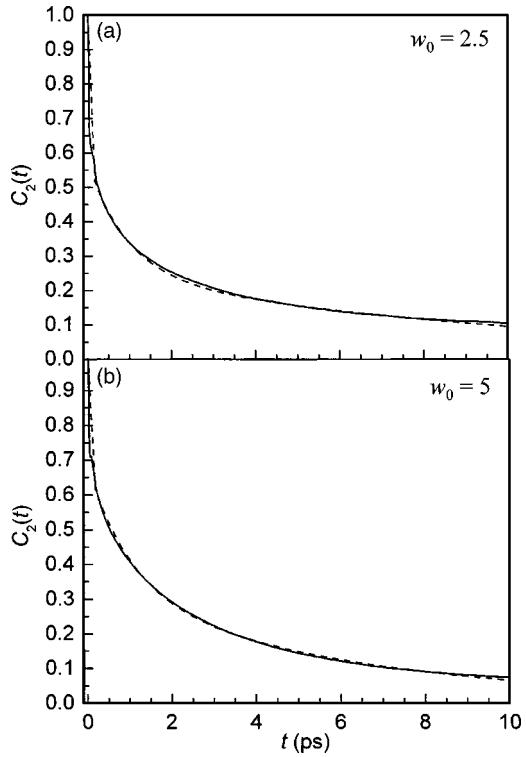

FIG. 4. MD simulations of the orientational dynamics $[C_2(t)]$ of water in AOT reverse micelles (Ref. 27) and triexponential fits (see Tables IV and V).

sembles, one associated with the head groups and one for the core waters, the same basic shapes of the curves were obtained, but with the head group subensemble displaying somewhat slower dynamics and the core subensemble somewhat faster dynamics than the curves displayed in Fig. 4. (Ref. 27) Therefore, the highly nonexponential shapes of the curves are not a result of two subensembles, each giving rise to different exponential decay curves.

$C_2(t)$ is directly related to $r(t)$, the orientational anisotropy measured here [see Eq. (2)]. The simulations were fit with a triexponential function constrained to have the sum of the three amplitude factors, α_i, equal unity (dashed curves). While not perfect, the triexponential function does a good job of reproducing the simulations, and the resulting parameters permit direct comparisons to the experimental results. The fit parameters for the three exponentials are given in Table IV. τ_1 and τ_2 are directly comparable to the measured values given in Table II. α_1 and α_2 are the equivalent of multiplying A_1 and A_2 of Table II by 2.5. The simulations give τ_{in} the inertial decay constant as ~40 fs. τ_{in} was not measurable in the experiments, but the simulation values are consistent with the observation that the inertial component has completely decayed by 200 fs. The amplitudes of the inertial components α_{in} can be compared to the measured values, which are $1-2.5(A_1+A_2)$ from Table II.

TABLE IV. Simulation orientational correlation function decay parameters.

Sample	α_{in}	τ_{in} (ps)	α_1	τ_1 (ps)	α_2	τ_2 (ps)
$w_0=2.5$	0.43	0.038	0.32	0.95	0.25	10.5
$w_0=5$	0.33	0.036	0.35	1.05	0.32	6.3

TABLE V. Simulation cone angles and diffusion constants.

Sample	θ_{in}	θ_{tot}	D_c^{-1} (ps)	D_m^{-1} (ps)
$w_0=2.5$	34°	52°	8	63
$w_0=5$	29°	48°	11	38

Qualitatively, the simulations of $w_0=2.5$ and 5 reverse micelles have the same general characteristics as the experimental results on $w_0=2$ and 5. There is a very fast inertial decay followed by a biexponential decay that has an ~1-ps decay time and then a significantly longer decay time. To make a more quantitative comparison between the MD simulations and the experimental results, the simulated data were analyzed in the identical manner as the experimental data. Table V presents the results. The simulations give inertial cone angles θ_{in} that are ~50% greater than the experimental values, and the total cone angles θ_{tot} are 50%–100% larger. The simulated inverse wobbling-in-a-cone diffusion constants D_c^{-1} are factors of 3–5 faster. They are consistent with experiment in that there is not a substantial change with w_0. The inverse diffusion constant for the final complete orientational relaxation D_m^{-1} have the correct trend in that the diffusion becomes significantly faster as the water nanopool becomes larger, but the times are too fast by factors of 3–7. Generally, the simulations show cone angles that are too large and diffusion that is too fast. One feature of the simulations that may be responsible for the quantitative differences with experiment is the lack of a detailed molecular model of the head groups.[27,32] While the agreement between the simulations and the experimental results is only semiquantitative, all of the basic features of the experiments are reproduced in the simulations, the trends are correct, and the actual numbers are in reasonable accord with the experiment given the difficulty of the simulations. This feature of having a biexponential decay in the orientational correlation is also present in the MD simulations of water molecule in a perfluro polyether reverse micelle system with a size of $w_0=8.4$.[49] Another important aspect of the simulations by Faeder and co-worker[32] is that they show that the counter ions (Na^+) are essentially fully associated with the negatively charged head groups. Therefore, the ionic strength of the water nanopools is low and not responsible for differences in orientational dynamics between the water confined in the reverse micelles and bulk water. Furthermore, pump-probe anisotropy experiments on salt solutions suggest that there is little effect on the orientational dynamics of bulk water beyond the first solvation shell of the ions.[50] IR pump-probe experiments that measured the lifetimes and orientational relaxation of a small probe molecule in nonionic reverse micelles showed significant differences from bulk water and a size dependence.[23,24] The experiments on nonionic reverse micelles support the results of the simulations that show that confinement rather than the influence of free ions in AOT reverse micelles is responsible for the trends seen here in both the experiments and simulations.

IV. CONCLUDING REMARKS

We have presented frequency-resolved pump-probe anisotropy experiments on the OD stretch of dilute HOD in water confined on a nanometer length scale in AOT reverse micelles. The experiments examined the influence of nanoscopic confinement on the orientational dynamics of water as a function of the water nanopool size, and the results were compared to identical measurements on bulk water. The experimental results are also compared to MD simulations of orientational relaxation in AOT reverse micelles.[27,32] Orientational relaxation in bulk water occurs as a single diffusive process (single exponential decay of the anisotropy) that results in complete orientational relaxation following, at most, a small initial very fast inertial decay. In contrast, the orientational diffusion in the confined water exhibits pronounced nonexponential decay of the anisotropy. Following a very fast inertial decay component of substantial amplitude, there is a decay on an ~1-ps time scale and another decay on tens of picosecond time scale (see Table II). The nonexponential decay is analyzed using a wobbling-in-a-cone model.[31] The diffusive cone angle decreases and the diffusion in the cone slows as the water nanopool size decreases (see Table III). The final diffusion that leads to complete orientational relaxation slows substantially as the nanopool becomes smaller (see Table III). The MD simulations[32] show the same trends, a very fast inertial decay followed by a longer time scale nonexponential decay (See Fig. 4 and Tables IV and V). While the trends in the MD simulations are similar to the experimental results, the cone angles are too large and both the cone diffusion constants and the final complete diffusion constants are too fast.

In the data analysis, the water molecules were treated as belonging to a single ensemble. However, as discussed briefly above, the MD simulations examined two classes of water molecules, those in the core of the reverse micelles and those that are associated with the head groups. The MD simulations indicate that the dynamics are different for these two subensembles of water molecules. The experiments have also addressed the issue of different classes of water molecules in reverse micelles.[16–18] The pump-probe data reported here, although measured at the peak of the absorption spectrum of each sample, may be a superposition of more than one ensemble. The postulated different subensembles of water might be expected to have different absorption frequencies,[16] which would suggest that the pump-probe anisotropy experiments may be frequency dependent. The preliminary wavelength selective vibrational echo experiments show that there is some frequency dependence for the OD stretch spectral diffusion.[29,30] Further experiments are being conducted to investigate the frequency dependence of the pump-probe anisotropy decays in the reverse micelle samples. More detailed frequency selective experiments may allow us to delineate the contributions to the observed orientation correlation function and to obtain separate orientation correlation functions for the different subensembles.

It is apparent from Fig. 3 and Tables II and III that the dynamics of water in $w_0=10$ reverse micelles are not bulklike. The linear optical spectroscopy on the OH stretch of water in reverse micelles has suggested that by $w_0=16$, the water in the nanopools behaves like the bulk water,[51] while measurements on the OH librational band indicates that water does not attain bulklike characteristics for w_0 between 20 and 40.[18] We are in the process of performing experiments on larger reverse micelles than those studied here using isooctane as a solvent to determine at what size the orientational dynamics of water in reverse micelles becomes equivalent to that of bulk water.

ACKNOWLEDGMENTS

We are grateful to Professor Branka Ladanyi, Department of Chemistry, Colorado State University at Fort Collins, for providing us with the molecular-dynamics simulation data presented in Fig. 4.[27] This work was supported by the Department of Energy (Grant No. DE-FG03-84ER1325I), the National Institutes of Health (Grant No. 2R01GM061137-05), and the National Science Foundation (Grant No. DMR-0332692).

APPENDIX: MODIFICATION OF THE WOBBLING-IN-THE-CONE ORIENTATION CORRELATION FUNCTION

Equation (4) describes the time-dependent anisotropy of a restricted rotor.[31] It consists of an overall unrestricted molecular reorientation governed by τ_m and the restricted diffusion in a cone parameterized by variables τ_c and Q^2. These two processes are assumed to be independent of each other.

In the experiments presented here, there are two cones, the inertial cone and the total cone. The cone angle for each is calculated with the same formula, Eq. (7). The restricted orientational relaxation can be viewed as a decay to a plateau. The value of the plateau gives the cone angle. In the normal wobbling in a cone, there is one plateau. In the absence of further orientational relaxation, the decay would be to a true plateau reflecting a spread of orientations to a specific nonrandom value. However, in the single cone case described in Eq. (4), the plateau decays with the final diffusion process that leads to complete orientational randomization.

When there are two cones, there are two plateaus. The inertial dynamics produces a decay to the first plateau. The decay from the first plateau is caused by diffusive wobbling in a cone that leads to the second plateau, which in turn decays by the final diffusion process. Equation (4) can be generalized to include an additional diffusion in a cone motion as

$$C_2(t) = [T^2 + (1 - T^2) \times \exp(-t/\tau_{\text{in}})][S^2 + (1 - S^2)\exp(-t/\tau_c)] \times \exp(-t/\tau_m), \tag{A1}$$

where T^2 and τ_{in} parameterize the first cone, in the experiments presented here the inertial cone, and S^2 and τ_c parameterize the second cone, the diffusive cone. As discussed in detail in the text, the orientational relaxation caused by the initial very fast inertial motion is not diffusive. However, it is so fast that its functional form is not measurable in the experiments and the simulations and fits presented in Fig. 4

show that the decay of the correlation function arising from the inertial motion can be fit reasonably well as a decaying exponential.

When Eq. (A1) is multiplied out, there are terms involving, $\exp[-(1/\tau_{\text{in}})-(1/\tau_m)]$, and $\exp[-(1/\tau_{\text{in}})-(1/\tau_c)-(1/\tau_m)]$. For the experiments discussed here $\tau_{\text{in}} \ll \tau_c, \tau_m$. τ_{in} is ~0.04 ps; τ_c is ~1 ps; and τ_m is ~10 ps. Therefore, it is an excellent approximation to replace the two exponentials given above with $\exp(-1/\tau_{\text{in}})$. With this approximation, Eq. (A1) reduces to

$$C_2(t) = (1 - T^2)\exp(-t/\tau_{\text{in}}) + T^2[S^2 + (1 - S^2) \times \exp(-t/\tau_c)]\exp(-t/\tau_m), \quad \text{(A2)}$$

which is Eq. (10) in the body of the paper.

[1] S. Habuchi, H. B. Kim, and N. Kitamura, Anal. Chem. **73**, 366 (2001).
[2] S. K. Pal and A. H. Zewail, Chem. Rev. (Washington, D.C.) **104**, 2099 (2004).
[3] R. Sutton and G. Sposito, J. Colloid Interface Sci. **237**, 174 (2001).
[4] R. Biswas and S. K. Pal, Chem. Phys. Lett. **387**, 221 (2004).
[5] M. P. Pileni, J. Phys. Chem. **97**, 6961 (1993).
[6] P. Schuster, G. Zundel, and C. Sandorfy, *The Hydrogen Bond: Recent Developments in Theory and Experiments* (North Holland, Amsterdam, 1976).
[7] H. J. Bakker, H. K. Neinhuys, G. Gallot, N. Lascoux, G. M. Gale, J. C. Leicknam, and S. Bratos, J. Chem. Phys. **116**, 2592 (2002).
[8] J. Stenger, D. Madsen, P. Hamm, E. T. J. Nibbering, and T. Elsaesser, J. Phys. Chem. A **106**, 2341 (2002).
[9] S. Yeremenko, M. S. Pshenichnikov, and D. A. Wiersma, Chem. Phys. Lett. **369**, 107 (2003).
[10] C. J. Fecko, J. D. Eaves, J. J. Loparo, A. Tokmakoff, and P. L. Geissler, Science **301**, 1698 (2003).
[11] E. T. J. Nibbering and T. Elsaesser, Chem. Rev. (Washington, D.C.) **104**, 1887 (2004).
[12] J. B. Asbury, T. Steinel, C. Stromberg, S. A. Corcelli, C. P. Lawrence, J. L. Skinner, and M. D. Fayer, J. Phys. Chem. A **108**, 1107 (2004).
[13] C. P. Lawrence and J. L. Skinner, J. Chem. Phys. **118**, 264 (2003).
[14] K. B. Møller, R. Rey, and J. T. Hynes, J. Phys. Chem. A **108**, 1275 (2004).
[15] N. E. Levinger, Science **298**, 1722 (2002).
[16] G. Onori and A. Santucci, J. Phys. Chem. **97**, 5430 (1993).
[17] L. P. Novaki and O. A. El Seoud, J. Colloid Interface Sci. **202**, 391 (1998).
[18] D. S. Venables, K. Huang, and C. A. Schmuttenmaer, J. Phys. Chem. B **105**, 9132 (2001).
[19] J. E. Boyd, A. Briskman, V. L. Colvin, and D. M. Mittleman, Phys. Rev. Lett. **87**, 147401 (2001).
[20] R. E. Riter, D. M. Willard, and N. E. Levinger, J. Phys. Chem. B **102**, 2705 (1998).
[21] N. E. Levinger, Curr. Opin. Colloid Interface Sci. **5**, 118 (2000).
[22] Q. Zhong, A. P. Baronavski, and J. C. Owrutsky, J. Chem. Phys. **118**, 7074 (2003).
[23] Q. Zhong, A. P. Baronavski, and J. C. Owrutsky, J. Chem. Phys. **119**, 9171 (2003).
[24] G. M. Sando, K. Dahl, and J. C. Owrutsky, J. Phys. Chem. A **108**, 11209 (2004).
[25] T. Patzlaff, M. Janich, G. Seifert, and H. Graener, Chem. Phys. **261**, 381 (2000).
[26] J. C. Deàk, Y. Pang, T. D. Sechler, Z. Wang, and D. D. Dlott, Science **306**, 473 (2004).
[27] M. R. Harpham, B. M. Ladanyi, N. E. Levinger, and K. W. Herwig, Chem. Phys. **121**, 7855 (2004).
[28] H. Maekawa, K. Ohta, and K. Tominaga, presented at the Mater. Res. Soc. Symp. Proc. 2004, 6.7.1-11.
[29] H.-S. Tan, I. R. Piletic, R. E. Riter, N. E. Levinger, and M. D. Fayer, Phys. Rev. Lett. **94**, 057405 (2005).
[30] I. R. Piletic, H.-S. Tan, and M. D. Fayer, J. Phys. Chem. A (submitted).
[31] G. Lipari and A. Szabo, Biophys. J. **30**, 489 (1980).
[32] J. Faeder and B. M. Ladanyi, J. Phys. Chem. B **104**, 1033 (2000).
[33] R. Trebino, K. W. DeLong, D. N. Fittinghoff, J. N. Sweetser, M. A. Krumbugel, B. A. Richman, and D. J. Kane, Rev. Sci. Instrum. **68**, 3277 (1997).
[34] S. Woutersen and H. J. Bakker, Nature (London) **402**, 507 (1999).
[35] K. J. Gaffney, I. R. Piletic, and M. D. Fayer, J. Chem. Phys. **118**, 2270 (2003).
[36] T. Kinugasa, A. Kondo, S. Nishimura, Y. Miyauchi, Y. Nishii, K. Watanabe, and H. Takeuchi, Colloids Surf., A **204**, 193 (2002).
[37] T. Tao, Biopolymers **8**, 609 (1969).
[38] A. Tokmakoff, J. Chem. Phys. **105**, 1 (1996).
[39] T. Steinel, J. B. Asbury, J. Zheng, and M. D. Fayer, J. Phys. Chem. A **108**, 10957 (2004).
[40] T. Steinel, J. B. Asbury, J. Zheng, and M. D. Fayer (unpublished). The value of 1.5 ps previously reported by the same authors was in error because of depolarization caused by optical elements in the experimental setup.
[41] J. J. Loparo, C. J. Fecko, J. D. Eaves, S. T. Roberts, and A. Tokmakoff, Phys. Rev. B **70**, 180201 (2004).
[42] C. C. Wang and R. Pecora, J. Chem. Phys. **72**, 5333 (1980).
[43] R. S. Berry, S. A. Rice, and J. Ross, *Physical Chemistry*, 2nd ed. (Oxford University Press, New York, 2000).
[44] P. Debye, *Polar Molecules* (Dover, New York, 1945).
[45] A. Maitra, J. Phys. Chem. **88**, 5122 (1984).
[46] *CRC Handbook of Chemistry and Physics*, 51st ed. edited by R. C. Weast (CRC, Cleveland, FL, 1970).
[47] A. Luzar and D. Chandler, J. Chem. Phys. **98**, 8160 (1993).
[48] J. B. Asbury, T. Steinel, K. Kwak, S. Corcelli, C. P. Lawrence, J. L. Skinner, and M. D. Fayer, J. Phys. Chem. A **121**, 12431 (2004).
[49] S. Senapati and M. L. Berkowitz, J. Phys. Chem. A **108**, 9768 (2004).
[50] A. W. Omta, M. F. Kropman, S. Woutersen, and H. J. Bakker, Science **301**, 347 (2003).
[51] Q. Li, S. F. Weng, J. G. Wu, and N. F. Zhou, J. Phys. Chem. B **102**, 3168 (1998).